Journal of Catalysis 271 (2010) iii–ix

Contents lists available at ScienceDirect

Journal of Catalysis

journal homepage: www.elsevier.com/locate/jcat

Journal of Catalysis Vol. 271, Issue 2, 2010

Contents

PRIORITY COMMUNICATION

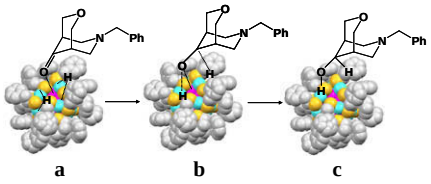

Atomically monodisperse $Au_{25}(SR)_{18}$ (R=CH_2CH_2Ph) nanoparticles are explored as a new type of stereoselective catalyst for hydrogenation of cyclic ketone to a specific isomer of the cyclic alcohol product. A complete (100%) stereoselectivity is obtained and the catalytic performance is further correlated with the crystal structure of the $Au_{25}(SR)_{18}$ nanoparticle.

REGULAR ARTICLES

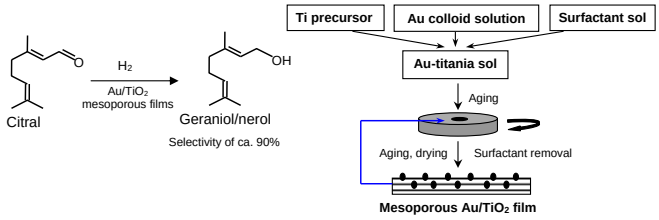

Control of the thickness of mesoporous Au/TiO_2 films was achieved by multiple spin-coating. A 300 nm thick Au-containing film showed high initial TOF of 1.4 s^{-1} and a selectivity towards unsaturated alcohols as high as 90% in the hydrogenation of citral.

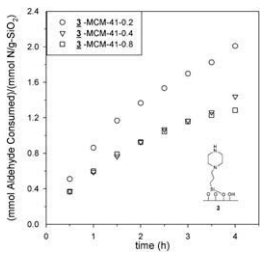

Amine-functionalized amine-MCM-41 materials were investigated as catalysts for the nitroaldol reaction. The secondary amines investigated were generally more active than primary amines.

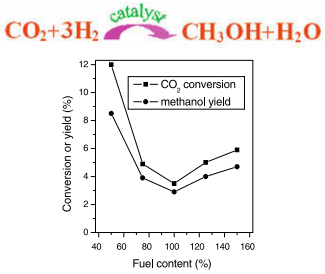

The fuel content used for the preparation of CuO–ZnO–ZrO_2 catalysts by combustion method had significant effect on CO_2 conversion and methanol yield for the synthesis of methanol from CO_2 hydrogenation.

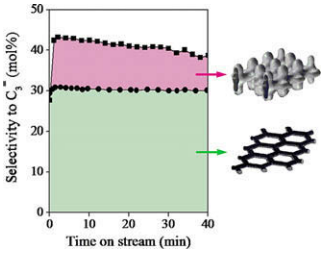

The contribution of 2-D sinusoidal 10-ring channels in H-MCM-22 to the overall MTO performance of this medium-pore zeolite was found to be considerably greater than that of its cylindrical supercages.

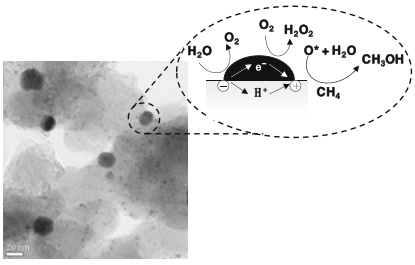

An electrochemical reactor for direct methanol synthesis from methane is downsized from macro- to micro- or nanoscale and operated without the need for an electrical power source.

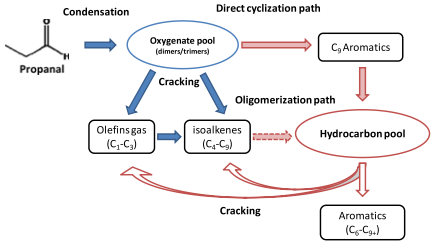

Propanal is found to be much more reactive than propylene and to form mostly 2-methyl-2-pentenal and C_9 aromatics as early products in the reaction network through the aldol pathway.

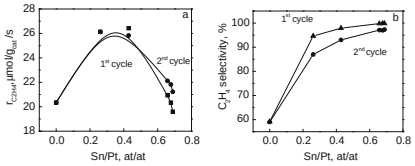

The effects of Sn on the dehydrogenation of ethane on Pt supported on calcined hydrotalcite (Pt/Mg(Al)O) were investigated. Sn was found to form an alloy with Pt and to enhance ethene selectivity and decrease coke deposition. Adsorption of ethene was identified as the primary source of CH_x (x = 1–3) species that are precursors to the formation of methane and coke.

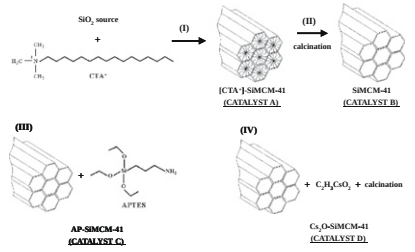

For the first time, the basicity of Si–MCM-41 mesoporous materials was compared with the as-synthesized material [CTA^+]–Si–MCM-41 (CTA^+ stands for the structure directing agent).

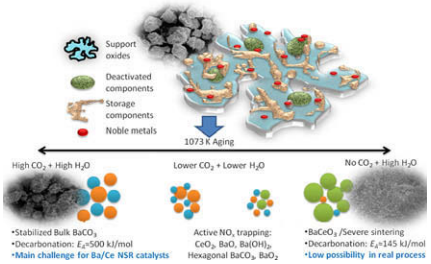

NO_x storage/reduction catalysts based on barium and cerium oxides were treated under different aging atmospheres to reveal the effects of CO_2 and steam on the chemical and morphological properties of the materials.

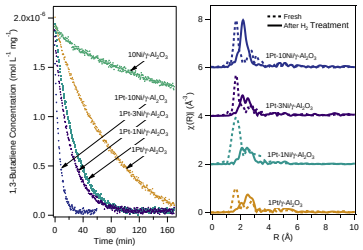

Hydrogenation activity was found to correlate to the extent of Pt–Ni bimetallic bond formation, as characterized by the coordination numbers obtained through EXAFS analysis of the Pt L_{III}-edge.

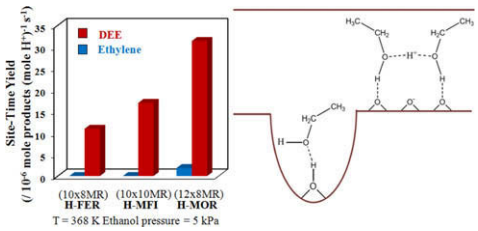

In zeolite pores large enough to accommodate ethanol dimers, ethanol preferentially dehydrates via a bimolecular pathway to generate diethyl ether since the formation of ethanol dimeric species is energetically more favorable than the formation of ethanol monomers. In zeolite channels too small to accommodate ethanol dimers, ethanol is selectively dehydrated via a unimolecular reaction pathway to generate ethylene.

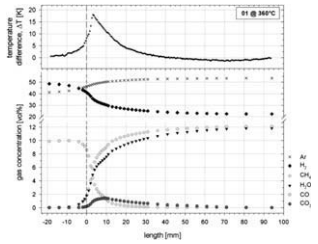

Spatially resolved gas concentration and catalyst temperature measurements in an optically accessible catalytic plate reactor allowed determining the kinetics of the exothermic CO methanation reaction with high initial CO partial pressure.

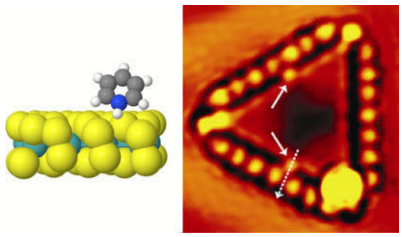

Inhibition of catalytic hydrodesulfurization activity is related to pyridinium species that are directly observed to adsorb strongly on the edges of MoS_2 nanoclusters.

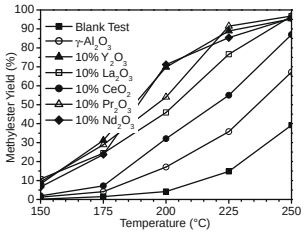

Pure rare earth oxides, supported rare earth oxides, and stoichiometric rare earth mixed oxide catalysts were used for the transesterification of different oils and fats with methanol. Structure–activity relationships are depicted.

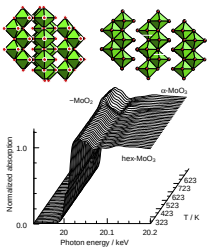

Molybdenum oxide supported on hollow vapor-grown carbon nanofibers is active in oxidation of propene to acrylic acid. In situ XAS under reaction conditions showed structural transformation from hex-MoO_3 to α-MoO_3.

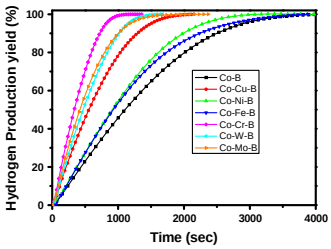

Cr-, W-, Mo-, and Cu-doped Co–B catalyst showed 3–4 times increment in H_2 generation rate when compared to the undoped catalyst for hydrolysis of $NaBH_4$ at 298 K, while Ni and Fe are only able to create a marginal increment in the catalytic performance.

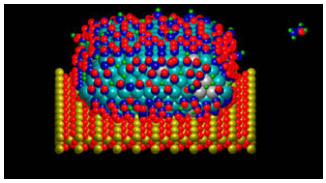

Combining experimental measurements with first-principles-based kinetic Monte Carlo modeling, the reaction kinetics of ethanol synthesis from CO hydrogenation over Rh/Mn/SiO_2 catalysts was studied. We find that addition of Mn promoter into Rh-based catalysts can lower CO insertion barriers thus improving the selectivity toward ethanol and other C_2^+ oxygenates. The effects of various promoters (M = Ir, Ga, V, Ti, Sc, Ca, and Li) on CO insertion step over Rh/M alloy nanoparticles were further investigated, suggesting that alloying the promoter with the electronegativity difference, $\Delta\chi$ = 0.7, between the promoter M and Rh is the most effective in lowering CO insertion barriers which leads to higher selectivity to ethanol.

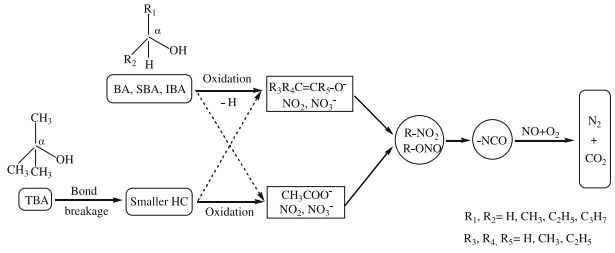

The presence of α-H is prerequisite for enolic species formation during NOx reduction by C4 alcohols over Ag/Al_2O_3, playing a crucial role in the efficiency for NOx conversion.

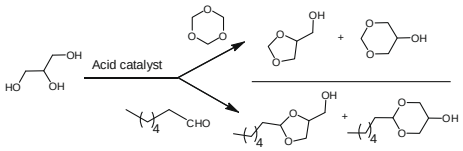

Gold salts and complexes are superior catalysts than other homo- and heterogeneous Brønsted and Lewis acids for obtaining valuable acetals from glycerol.

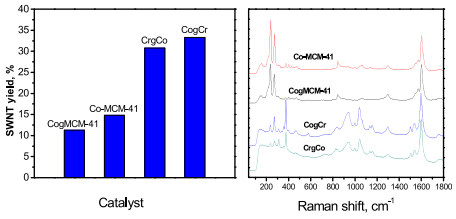

Characterization of SWNT synthesized on various catalytic systems: Co grafted on MCM-41 (CogMCM-41), Co incorporated on MCM-41 (Co–MCM-41), Cr grafted on Co–MCM-41 (CrgCo) and Co grafted on Cr–MCM-41 (CogCr). Left – resultant SWNT yield. Right – Resonant Raman Spectroscopy of SWNT.

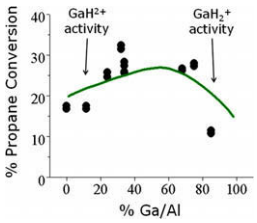

Unified gallium monohydride–gallium dihydride model predictions, indicating the regions where each active site dominates. All aluminum assumed to be in pairs, Si/Al = 16, T = 520 °C, space time = 1.514 g_{cat} h/mol.

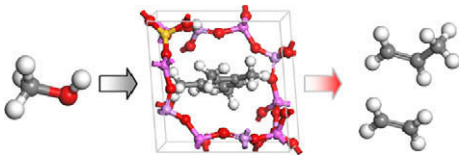

Theoretical calculations on the methanol-to-olefins conversion in HSAPO-34 reveal that hexamethylbenzene and pentamethylbenzene are not more active than methylbenzenes with fewer methyl groups, and propene is the favored product.

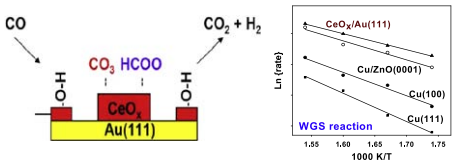

Water–gas shift reaction over an inverse CeO_x/Au(1 1 1) catalyst: activity and relative stability of possible reaction intermediates (HO, HCOO and CO_3).

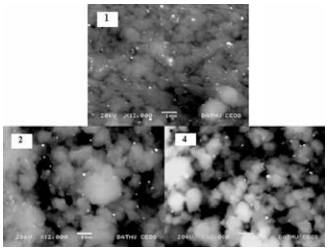

Backscattered scanning electron microscopy images of PtH-MFI-40 catalysts: Fresh (1), 4 h (2), and 48 h (4) on-stream.

RESEARCH NOTE

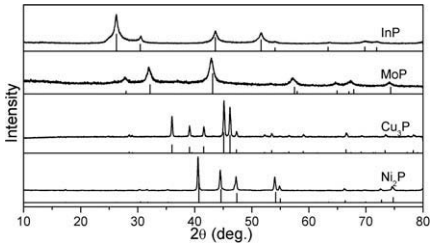

This approach uses metal oxide as precursors. Both bulk metal phosphides with special morphology and supported metal phosphides that are used as catalysts can be synthesized by this synthetic approach.